EUROPEAN ORGANIZATION FOR NUCLEAR RESEARCH (CERN)

CERN-PH-EP-2014-055
LHCb-PAPER-2014-006
31 March 2014

arXiv:1403.8044v2 [hep-ex] 1 Apr 2014

Differential branching fractions and isospin asymmetries of $B \to K^{(*)}\mu^+\mu^-$ decays

The LHCb collaboration[†]

Abstract

The isospin asymmetries of $B \to K\mu^+\mu^-$ and $B \to K^*\mu^+\mu^-$ decays and the partial branching fractions of the $B^0 \to K^0\mu^+\mu^-$, $B^+ \to K^+\mu^+\mu^-$ and $B^+ \to K^{*+}\mu^+\mu^-$ decays are measured as functions of the dimuon mass squared, q^2. The data used correspond to an integrated luminosity of 3 fb^{-1} from proton-proton collisions collected with the LHCb detector at centre-of-mass energies of 7 TeV and 8 TeV in 2011 and 2012, respectively. The isospin asymmetries are both consistent with the Standard Model expectations. The three measured branching fractions, while individually consistent, all favour lower values than their respective Standard Model predictions.

Submitted to JHEP

© CERN on behalf of the LHCb collaboration, license CC-BY-3.0.

[†]Authors are listed on the following pages.

LHCb collaboration

R. Aaij[41], B. Adeva[37], M. Adinolfi[46], A. Affolder[52], Z. Ajaltouni[5], J. Albrecht[9], F. Alessio[38], M. Alexander[51], S. Ali[41], G. Alkhazov[30], P. Alvarez Cartelle[37], A.A. Alves Jr[25,38], S. Amato[2], S. Amerio[22], Y. Amhis[7], L. An[3], L. Anderlini[17,g], J. Anderson[40], R. Andreassen[57], M. Andreotti[16,f], J.E. Andrews[58], R.B. Appleby[54], O. Aquines Gutierrez[10], F. Archilli[38], A. Artamonov[35], M. Artuso[59], E. Aslanides[6], G. Auriemma[25,n], M. Baalouch[5], S. Bachmann[11], J.J. Back[48], A. Badalov[36], V. Balagura[31], W. Baldini[16], R.J. Barlow[54], C. Barschel[38], S. Barsuk[7], W. Barter[47], V. Batozskaya[28], Th. Bauer[41], A. Bay[39], J. Beddow[51], F. Bedeschi[23], I. Bediaga[1], S. Belogurov[31], K. Belous[35], I. Belyaev[31], E. Ben-Haim[8], G. Bencivenni[18], S. Benson[50], J. Benton[46], A. Berezhnoy[32], R. Bernet[40], M.-O. Bettler[47], M. van Beuzekom[41], A. Bien[11], S. Bifani[45], T. Bird[54], A. Bizzeti[17,i], P.M. Bjørnstad[54], T. Blake[48], F. Blanc[39], J. Blouw[10], S. Blusk[59], V. Bocci[25], A. Bondar[34], N. Bondar[30,38], W. Bonivento[15,38], S. Borghi[54], A. Borgia[59], M. Borsato[7], T.J.V. Bowcock[52], E. Bowen[40], C. Bozzi[16], T. Brambach[9], J. van den Brand[42], J. Bressieux[39], D. Brett[54], M. Britsch[10], T. Britton[59], N.H. Brook[46], H. Brown[52], A. Bursche[40], G. Busetto[22,q], J. Buytaert[38], S. Cadeddu[15], R. Calabrese[16,f], O. Callot[7], M. Calvi[20,k], M. Calvo Gomez[36,o], A. Camboni[36], P. Campana[18,38], D. Campora Perez[38], A. Carbone[14,d], G. Carboni[24,l], R. Cardinale[19,38,j], A. Cardini[15], H. Carranza-Mejia[50], L. Carson[50], K. Carvalho Akiba[2], G. Casse[52], L. Cassina[20], L. Castillo Garcia[38], M. Cattaneo[38], Ch. Cauet[9], R. Cenci[58], M. Charles[8], Ph. Charpentier[38], S.-F. Cheung[55], N. Chiapolini[40], M. Chrzaszcz[40,26], K. Ciba[38], X. Cid Vidal[38], G. Ciezarek[53], P.E.L. Clarke[50], M. Clemencic[38], H.V. Cliff[47], J. Closier[38], C. Coca[29], V. Coco[38], J. Cogan[6], E. Cogneras[5], P. Collins[38], A. Comerma-Montells[11], A. Contu[15,38], A. Cook[46], M. Coombes[46], S. Coquereau[8], G. Corti[38], M. Corvo[16,f], I. Counts[56], B. Couturier[38], G.A. Cowan[50], D.C. Craik[48], M. Cruz Torres[60], S. Cunliffe[53], R. Currie[50], C. D'Ambrosio[38], J. Dalseno[46], P. David[8], P.N.Y. David[41], A. Davis[57], K. De Bruyn[41], S. De Capua[54], M. De Cian[11], J.M. De Miranda[1], L. De Paula[2], W. De Silva[57], P. De Simone[18], D. Decamp[4], M. Deckenhoff[9], L. Del Buono[8], N. Déléage[4], D. Derkach[55], O. Deschamps[5], F. Dettori[42], A. Di Canto[38], H. Dijkstra[38], S. Donleavy[52], F. Dordei[11], M. Dorigo[39], A. Dosil Suárez[37], D. Dossett[48], A. Dovbnya[43], F. Dupertuis[39], P. Durante[38], R. Dzhelyadin[35], A. Dziurda[26], A. Dzyuba[30], S. Easo[49], U. Egede[53], V. Egorychev[31], S. Eidelman[34], S. Eisenhardt[50], U. Eitschberger[9], R. Ekelhof[9], L. Eklund[51,38], I. El Rifai[5], Ch. Elsasser[40], S. Esen[11], T. Evans[55], A. Falabella[16,f], C. Färber[11], C. Farinelli[41], S. Farry[52], D. Ferguson[50], V. Fernandez Albor[37], F. Ferreira Rodrigues[1], M. Ferro-Luzzi[38], S. Filippov[33], M. Fiore[16,f], M. Fiorini[16,f], M. Firlej[27], C. Fitzpatrick[38], T. Fiutowski[27], M. Fontana[10], F. Fontanelli[19,j], R. Forty[38], O. Francisco[2], M. Frank[38], C. Frei[38], M. Frosini[17,38,g], J. Fu[21,38], E. Furfaro[24,l], A. Gallas Torreira[37], D. Galli[14,d], S. Gallorini[22], S. Gambetta[19,j], M. Gandelman[2], P. Gandini[59], Y. Gao[3], J. Garofoli[59], J. Garra Tico[47], L. Garrido[36], C. Gaspar[38], R. Gauld[55], L. Gavardi[9], E. Gersabeck[11], M. Gersabeck[54], T. Gershon[48], Ph. Ghez[4], A. Gianelle[22], S. Giani'[39], V. Gibson[47], L. Giubega[29], V.V. Gligorov[38], C. Göbel[60], D. Golubkov[31], A. Golutvin[53,31,38], A. Gomes[1,a], H. Gordon[38], C. Gotti[20], M. Grabalosa Gándara[5], R. Graciani Diaz[36], L.A. Granado Cardoso[38], E. Graugés[36], G. Graziani[17], A. Grecu[29], E. Greening[55], S. Gregson[47], P. Griffith[45], L. Grillo[11], O. Grünberg[62], B. Gui[59], E. Gushchin[33], Yu. Guz[35,38], T. Gys[38], C. Hadjivasiliou[59], G. Haefeli[39], C. Haen[38], S.C. Haines[47], S. Hall[53], B. Hamilton[58], T. Hampson[46], X. Han[11], S. Hansmann-Menzemer[11], N. Harnew[55], S.T. Harnew[46], J. Harrison[54], T. Hartmann[62], J. He[38], T. Head[38], V. Heijne[41], K. Hennessy[52], P. Henrard[5], L. Henry[8],

J.A. Hernando Morata[37], E. van Herwijnen[38], M. Heß[62], A. Hicheur[1], D. Hill[55], M. Hoballah[5], C. Hombach[54], W. Hulsbergen[41], P. Hunt[55], N. Hussain[55], D. Hutchcroft[52], D. Hynds[51], M. Idzik[27], P. Ilten[56], R. Jacobsson[38], A. Jaeger[11], J. Jalocha[55], E. Jans[41], P. Jaton[39], A. Jawahery[58], M. Jezabek[26], F. Jing[3], M. John[55], D. Johnson[55], C.R. Jones[47], C. Joram[38], B. Jost[38], N. Jurik[59], M. Kaballo[9], S. Kandybei[43], W. Kanso[6], M. Karacson[38], T.M. Karbach[38], M. Kelsey[59], I.R. Kenyon[45], T. Ketel[42], B. Khanji[20], C. Khurewathanakul[39], S. Klaver[54], O. Kochebina[7], M. Kolpin[11], I. Komarov[39], R.F. Koopman[42], P. Koppenburg[41,38], M. Korolev[32], A. Kozlinskiy[41], L. Kravchuk[33], K. Kreplin[11], M. Kreps[48], G. Krocker[11], P. Krokovny[34], F. Kruse[9], M. Kucharczyk[20,26,38,k], V. Kudryavtsev[34], K. Kurek[28], T. Kvaratskheliya[31], V.N. La Thi[39], D. Lacarrere[38], G. Lafferty[54], A. Lai[15], D. Lambert[50], R.W. Lambert[42], E. Lanciotti[38], G. Lanfranchi[18], C. Langenbruch[38], B. Langhans[38], T. Latham[48], C. Lazzeroni[45], R. Le Gac[6], J. van Leerdam[41], J.-P. Lees[4], R. Lefèvre[5], A. Leflat[32], J. Lefrançois[7], S. Leo[23], O. Leroy[6], T. Lesiak[26], B. Leverington[11], Y. Li[3], M. Liles[52], R. Lindner[38], C. Linn[38], F. Lionetto[40], B. Liu[15], G. Liu[38], S. Lohn[38], I. Longstaff[51], J.H. Lopes[2], N. Lopez-March[39], P. Lowdon[40], H. Lu[3], D. Lucchesi[22,q], H. Luo[50], A. Lupato[22], E. Luppi[16,f], O. Lupton[55], F. Machefert[7], I.V. Machikhiliyan[31], F. Maciuc[29], O. Maev[30], S. Malde[55], G. Manca[15,e], G. Mancinelli[6], M. Manzali[16,f], J. Maratas[5], J.F. Marchand[4], U. Marconi[14], C. Marin Benito[36], P. Marino[23,s], R. Märki[39], J. Marks[11], G. Martellotti[25], A. Martens[8], A. Martín Sánchez[7], M. Martinelli[41], D. Martinez Santos[42], F. Martinez Vidal[64], D. Martins Tostes[2], A. Massafferri[1], R. Matev[38], Z. Mathe[38], C. Matteuzzi[20], A. Mazurov[16,f], M. McCann[53], J. McCarthy[45], A. McNab[54], R. McNulty[12], B. McSkelly[52], B. Meadows[57,55], F. Meier[9], M. Meissner[11], M. Merk[41], D.A. Milanes[8], M.-N. Minard[4], J. Molina Rodriguez[60], S. Monteil[5], D. Moran[54], M. Morandin[22], P. Morawski[26], A. Mordà[6], M.J. Morello[23,s], J. Moron[27], R. Mountain[59], F. Muheim[50], K. Müller[40], R. Muresan[29], B. Muster[39], P. Naik[46], T. Nakada[39], R. Nandakumar[49], I. Nasteva[2], M. Needham[50], N. Neri[21], S. Neubert[38], N. Neufeld[38], M. Neuner[11], A.D. Nguyen[39], T.D. Nguyen[39], C. Nguyen-Mau[39,p], M. Nicol[7], V. Niess[5], R. Niet[9], N. Nikitin[32], T. Nikodem[11], A. Novoselov[35], A. Oblakowska-Mucha[27], V. Obraztsov[35], S. Oggero[41], S. Ogilvy[51], O. Okhrimenko[44], R. Oldeman[15,e], G. Onderwater[65], M. Orlandea[29], J.M. Otalora Goicochea[2], P. Owen[53], A. Oyanguren[64], B.K. Pal[59], A. Palano[13,c], F. Palombo[21,t], M. Palutan[18], J. Panman[38], A. Papanestis[49,38], M. Pappagallo[51], C. Parkes[54], C.J. Parkinson[9], G. Passaleva[17], G.D. Patel[52], M. Patel[53], C. Patrignani[19,j], A. Pazos Alvarez[37], A. Pearce[54], A. Pellegrino[41], M. Pepe Altarelli[38], S. Perazzini[14,d], E. Perez Trigo[37], P. Perret[5], M. Perrin-Terrin[6], L. Pescatore[45], E. Pesen[66], K. Petridis[53], A. Petrolini[19,j], E. Picatoste Olloqui[36], B. Pietrzyk[4], T. Pilař[48], D. Pinci[25], A. Pistone[19], S. Playfer[50], M. Plo Casasus[37], F. Polci[8], A. Poluektov[48,34], E. Polycarpo[2], A. Popov[35], D. Popov[10], B. Popovici[29], C. Potterat[2], A. Powell[55], J. Prisciandaro[39], A. Pritchard[52], C. Prouve[46], V. Pugatch[44], A. Puig Navarro[39], G. Punzi[23,r], W. Qian[4], B. Rachwal[26], J.H. Rademacker[46], B. Rakotomiaramanana[39], M. Rama[18], M.S. Rangel[2], I. Raniuk[43], N. Rauschmayr[38], G. Raven[42], S. Reichert[54], M.M. Reid[48], A.C. dos Reis[1], S. Ricciardi[49], A. Richards[53], K. Rinnert[52], V. Rives Molina[36], D.A. Roa Romero[5], P. Robbe[7], A.B. Rodrigues[1], E. Rodrigues[54], P. Rodriguez Perez[54], S. Roiser[38], V. Romanovsky[35], A. Romero Vidal[37], M. Rotondo[22], J. Rouvinet[39], T. Ruf[38], F. Ruffini[23], H. Ruiz[36], P. Ruiz Valls[64], G. Sabatino[25,l], J.J. Saborido Silva[37], N. Sagidova[30], P. Sail[51], B. Saitta[15,e], V. Salustino Guimaraes[2], C. Sanchez Mayordomo[64], B. Sanmartin Sedes[37], R. Santacesaria[25], C. Santamarina Rios[37], E. Santovetti[24,l], M. Sapunov[6], A. Sarti[18,m], C. Satriano[25,n], A. Satta[24], M. Savrie[16,f], D. Savrina[31,32], M. Schiller[42], H. Schindler[38], M. Schlupp[9], M. Schmelling[10], B. Schmidt[38],

O. Schneider[39], A. Schopper[38], M.-H. Schune[7], R. Schwemmer[38], B. Sciascia[18], A. Sciubba[25], M. Seco[37], A. Semennikov[31], K. Senderowska[27], I. Sepp[53], N. Serra[40], J. Serrano[6], L. Sestini[22], P. Seyfert[11], M. Shapkin[35], I. Shapoval[16,43,f], Y. Shcheglov[30], T. Shears[52], L. Shekhtman[34], V. Shevchenko[63], A. Shires[9], R. Silva Coutinho[48], G. Simi[22], M. Sirendi[47], N. Skidmore[46], T. Skwarnicki[59], N.A. Smith[52], E. Smith[55,49], E. Smith[53], J. Smith[47], M. Smith[54], H. Snoek[41], M.D. Sokoloff[57], F.J.P. Soler[51], F. Soomro[39], D. Souza[46], B. Souza De Paula[2], B. Spaan[9], A. Sparkes[50], F. Spinella[23], P. Spradlin[51], F. Stagni[38], S. Stahl[11], O. Steinkamp[40], O. Stenyakin[35], S. Stevenson[55], S. Stoica[29], S. Stone[59], B. Storaci[40], S. Stracka[23,38], M. Straticiuc[29], U. Straumann[40], R. Stroili[22], V.K. Subbiah[38], L. Sun[57], W. Sutcliffe[53], K. Swientek[27], S. Swientek[9], V. Syropoulos[42], M. Szczekowski[28], P. Szczypka[39,38], D. Szilard[2], T. Szumlak[27], S. T'Jampens[4], M. Teklishyn[7], G. Tellarini[16,f], E. Teodorescu[29], F. Teubert[38], C. Thomas[55], E. Thomas[38], J. van Tilburg[41], V. Tisserand[4], M. Tobin[39], S. Tolk[42], L. Tomassetti[16,f], D. Tonelli[38], S. Topp-Joergensen[55], N. Torr[55], E. Tournefier[4], S. Tourneur[39], M.T. Tran[39], M. Tresch[40], A. Tsaregorodtsev[6], P. Tsopelas[41], N. Tuning[41], M. Ubeda Garcia[38], A. Ukleja[28], A. Ustyuzhanin[63], U. Uwer[11], V. Vagnoni[14], G. Valenti[14], A. Vallier[7], R. Vazquez Gomez[18], P. Vazquez Regueiro[37], C. Vázquez Sierra[37], S. Vecchi[16], J.J. Velthuis[46], M. Veltri[17,h], G. Veneziano[39], M. Vesterinen[11], B. Viaud[7], D. Vieira[2], M. Vieites Diaz[37], X. Vilasis-Cardona[36,o], A. Vollhardt[40], D. Volyanskyy[10], D. Voong[46], A. Vorobyev[30], V. Vorobyev[34], C. Voß[62], H. Voss[10], J.A. de Vries[41], R. Waldi[62], C. Wallace[48], R. Wallace[12], J. Walsh[23], S. Wandernoth[11], J. Wang[59], D.R. Ward[47], N.K. Watson[45], A.D. Webber[54], D. Websdale[53], M. Whitehead[48], J. Wicht[38], D. Wiedner[11], G. Wilkinson[55], M.P. Williams[45], M. Williams[56], F.F. Wilson[49], J. Wimberley[58], J. Wishahi[9], W. Wislicki[28], M. Witek[26], G. Wormser[7], S.A. Wotton[47], S. Wright[47], S. Wu[3], K. Wyllie[38], Y. Xie[61], Z. Xing[59], Z. Xu[39], Z. Yang[3], X. Yuan[3], O. Yushchenko[35], M. Zangoli[14], M. Zavertyaev[10,b], F. Zhang[3], L. Zhang[59], W.C. Zhang[12], Y. Zhang[3], A. Zhelezov[11], A. Zhokhov[31], L. Zhong[3], A. Zvyagin[38].

[1] *Centro Brasileiro de Pesquisas Físicas (CBPF), Rio de Janeiro, Brazil*
[2] *Universidade Federal do Rio de Janeiro (UFRJ), Rio de Janeiro, Brazil*
[3] *Center for High Energy Physics, Tsinghua University, Beijing, China*
[4] *LAPP, Université de Savoie, CNRS/IN2P3, Annecy-Le-Vieux, France*
[5] *Clermont Université, Université Blaise Pascal, CNRS/IN2P3, LPC, Clermont-Ferrand, France*
[6] *CPPM, Aix-Marseille Université, CNRS/IN2P3, Marseille, France*
[7] *LAL, Université Paris-Sud, CNRS/IN2P3, Orsay, France*
[8] *LPNHE, Université Pierre et Marie Curie, Université Paris Diderot, CNRS/IN2P3, Paris, France*
[9] *Fakultät Physik, Technische Universität Dortmund, Dortmund, Germany*
[10] *Max-Planck-Institut für Kernphysik (MPIK), Heidelberg, Germany*
[11] *Physikalisches Institut, Ruprecht-Karls-Universität Heidelberg, Heidelberg, Germany*
[12] *School of Physics, University College Dublin, Dublin, Ireland*
[13] *Sezione INFN di Bari, Bari, Italy*
[14] *Sezione INFN di Bologna, Bologna, Italy*
[15] *Sezione INFN di Cagliari, Cagliari, Italy*
[16] *Sezione INFN di Ferrara, Ferrara, Italy*
[17] *Sezione INFN di Firenze, Firenze, Italy*
[18] *Laboratori Nazionali dell'INFN di Frascati, Frascati, Italy*
[19] *Sezione INFN di Genova, Genova, Italy*
[20] *Sezione INFN di Milano Bicocca, Milano, Italy*
[21] *Sezione INFN di Milano, Milano, Italy*
[22] *Sezione INFN di Padova, Padova, Italy*
[23] *Sezione INFN di Pisa, Pisa, Italy*

[24] *Sezione INFN di Roma Tor Vergata, Roma, Italy*
[25] *Sezione INFN di Roma La Sapienza, Roma, Italy*
[26] *Henryk Niewodniczanski Institute of Nuclear Physics Polish Academy of Sciences, Kraków, Poland*
[27] *AGH - University of Science and Technology, Faculty of Physics and Applied Computer Science, Kraków, Poland*
[28] *National Center for Nuclear Research (NCBJ), Warsaw, Poland*
[29] *Horia Hulubei National Institute of Physics and Nuclear Engineering, Bucharest-Magurele, Romania*
[30] *Petersburg Nuclear Physics Institute (PNPI), Gatchina, Russia*
[31] *Institute of Theoretical and Experimental Physics (ITEP), Moscow, Russia*
[32] *Institute of Nuclear Physics, Moscow State University (SINP MSU), Moscow, Russia*
[33] *Institute for Nuclear Research of the Russian Academy of Sciences (INR RAN), Moscow, Russia*
[34] *Budker Institute of Nuclear Physics (SB RAS) and Novosibirsk State University, Novosibirsk, Russia*
[35] *Institute for High Energy Physics (IHEP), Protvino, Russia*
[36] *Universitat de Barcelona, Barcelona, Spain*
[37] *Universidad de Santiago de Compostela, Santiago de Compostela, Spain*
[38] *European Organization for Nuclear Research (CERN), Geneva, Switzerland*
[39] *Ecole Polytechnique Fédérale de Lausanne (EPFL), Lausanne, Switzerland*
[40] *Physik-Institut, Universität Zürich, Zürich, Switzerland*
[41] *Nikhef National Institute for Subatomic Physics, Amsterdam, The Netherlands*
[42] *Nikhef National Institute for Subatomic Physics and VU University Amsterdam, Amsterdam, The Netherlands*
[43] *NSC Kharkiv Institute of Physics and Technology (NSC KIPT), Kharkiv, Ukraine*
[44] *Institute for Nuclear Research of the National Academy of Sciences (KINR), Kyiv, Ukraine*
[45] *University of Birmingham, Birmingham, United Kingdom*
[46] *H.H. Wills Physics Laboratory, University of Bristol, Bristol, United Kingdom*
[47] *Cavendish Laboratory, University of Cambridge, Cambridge, United Kingdom*
[48] *Department of Physics, University of Warwick, Coventry, United Kingdom*
[49] *STFC Rutherford Appleton Laboratory, Didcot, United Kingdom*
[50] *School of Physics and Astronomy, University of Edinburgh, Edinburgh, United Kingdom*
[51] *School of Physics and Astronomy, University of Glasgow, Glasgow, United Kingdom*
[52] *Oliver Lodge Laboratory, University of Liverpool, Liverpool, United Kingdom*
[53] *Imperial College London, London, United Kingdom*
[54] *School of Physics and Astronomy, University of Manchester, Manchester, United Kingdom*
[55] *Department of Physics, University of Oxford, Oxford, United Kingdom*
[56] *Massachusetts Institute of Technology, Cambridge, MA, United States*
[57] *University of Cincinnati, Cincinnati, OH, United States*
[58] *University of Maryland, College Park, MD, United States*
[59] *Syracuse University, Syracuse, NY, United States*
[60] *Pontifícia Universidade Católica do Rio de Janeiro (PUC-Rio), Rio de Janeiro, Brazil, associated to* [2]
[61] *Institute of Particle Physics, Central China Normal University, Wuhan, Hubei, China, associated to* [3]
[62] *Institut für Physik, Universität Rostock, Rostock, Germany, associated to* [11]
[63] *National Research Centre Kurchatov Institute, Moscow, Russia, associated to* [31]
[64] *Instituto de Fisica Corpuscular (IFIC), Universitat de Valencia-CSIC, Valencia, Spain, associated to* [36]
[65] *KVI - University of Groningen, Groningen, The Netherlands, associated to* [41]
[66] *Celal Bayar University, Manisa, Turkey, associated to* [38]

[a] *Universidade Federal do Triângulo Mineiro (UFTM), Uberaba-MG, Brazil*
[b] *P.N. Lebedev Physical Institute, Russian Academy of Science (LPI RAS), Moscow, Russia*
[c] *Università di Bari, Bari, Italy*
[d] *Università di Bologna, Bologna, Italy*
[e] *Università di Cagliari, Cagliari, Italy*
[f] *Università di Ferrara, Ferrara, Italy*

[g] *Università di Firenze, Firenze, Italy*
[h] *Università di Urbino, Urbino, Italy*
[i] *Università di Modena e Reggio Emilia, Modena, Italy*
[j] *Università di Genova, Genova, Italy*
[k] *Università di Milano Bicocca, Milano, Italy*
[l] *Università di Roma Tor Vergata, Roma, Italy*
[m] *Università di Roma La Sapienza, Roma, Italy*
[n] *Università della Basilicata, Potenza, Italy*
[o] *LIFAELS, La Salle, Universitat Ramon Llull, Barcelona, Spain*
[p] *Hanoi University of Science, Hanoi, Viet Nam*
[q] *Università di Padova, Padova, Italy*
[r] *Università di Pisa, Pisa, Italy*
[s] *Scuola Normale Superiore, Pisa, Italy*
[t] *Università degli Studi di Milano, Milano, Italy*

1 Introduction

The rare decay of a B meson into a strange meson and a $\mu^+\mu^-$ pair is a $b \to s$ quark-level transition. In the Standard Model (SM), this can only proceed via loop diagrams. The loop-order suppression of the SM amplitudes increases the sensitivity to new virtual particles that can influence the decay amplitude at a similar level to the SM contribution. The branching fractions of $B \to K^{(*)}\mu^+\mu^-$ decays are highly sensitive to contributions from vector or axial-vector like particles predicted in extensions of the SM. However, despite recent progress in lattice calculations [1,2], theoretical predictions of the decay rates suffer from relatively large uncertainties in the $B \to K^{(*)}$ form factor calculations.

To maximise sensitivity, observables can be constructed from ratios or asymmetries where the leading form factor uncertainties cancel. The *CP*-averaged isospin asymmetry ($A_{\rm I}$) is such an observable. It is defined as

$$\begin{aligned} A_{\rm I} &= \frac{\Gamma(B^0 \to K^{(*)0}\mu^+\mu^-) - \Gamma(B^+ \to K^{(*)+}\mu^+\mu^-)}{\Gamma(B^0 \to K^{(*)0}\mu^+\mu^-) + \Gamma(B^+ \to K^{(*)+}\mu^+\mu^-)} \\ &= \frac{\mathcal{B}(B^0 \to K^{(*)0}\mu^+\mu^-) - (\tau_0/\tau_+)\cdot\mathcal{B}(B^+ \to K^{(*)+}\mu^+\mu^-)}{\mathcal{B}(B^0 \to K^{(*)0}\mu^+\mu^-) + (\tau_0/\tau_+)\cdot\mathcal{B}(B^+ \to K^{(*)+}\mu^+\mu^-)}, \end{aligned} \tag{1}$$

where $\Gamma(f)$ and $\mathcal{B}(f)$ are the partial width and branching fraction of the $B \to f$ decay and τ_0/τ_+ is the ratio of the lifetimes of the B^0 and B^+ mesons[1]. The decays in the isospin ratio differ only by the charge of the light (spectator) quark in the B meson. The SM prediction for $A_{\rm I}$ is $\mathcal{O}(1\%)$ in the dimuon mass squared, q^2, region below the J/ψ resonance [3–5]. There is no precise prediction for $A_{\rm I}$ for the q^2 region above the J/ψ resonance, but it is expected to be even smaller than at low q^2 [5]. As q^2 approaches zero, the isospin asymmetry of $B \to K^*\mu^+\mu^-$ is expected to approach the same asymmetry as in $B \to K^*\gamma$ decays, which is measured to be $(5 \pm 3)\%$ [6].

Previously, $A_{\rm I}$ has been measured by the BaBar [7], Belle [8] and LHCb [9] collaborations, where measurements for the $B \to K\mu^+\mu^-$ decay have predominantly given negative values of $A_{\rm I}$. In particular, the $B \to K\mu^+\mu^-$ isospin asymmetry measured by the LHCb experiment deviates from zero by over 4 standard deviations. For $B \to K^*\mu^+\mu^-$, measurements of $A_{\rm I}$ are consistent with zero.

This paper describes a measurement of the isospin asymmetry in $B \to K\mu^+\mu^-$ and $B \to K^*\mu^+\mu^-$ decays based on data collected with the LHCb detector, corresponding to an integrated luminosity of $1\,{\rm fb}^{-1}$ recorded in 2011 at a centre-of-mass energy $\sqrt{s} = 7$ TeV, and $2\,{\rm fb}^{-1}$ recorded in 2012 at $\sqrt{s} = 8$ TeV. The previous analysis [9] was carried out on the $1\,{\rm fb}^{-1}$ of data recorded in 2011. The analysis presented here includes, in addition to the data from 2012, a re-analysis of the full $1\,{\rm fb}^{-1}$ data sample with improved detector alignment parameters, reconstruction algorithms and event selection. Thus it supersedes the measurements in Ref. [9]. Moreover, the assumption that there is no isospin asymmetry in the $B \to J/\psi K^{(*)}$ decays is now used for all the measurements.

[1]The inclusion of charge conjugated processes is implied throughout this paper.

The isospin asymmetries are determined by measuring the differential branching fractions of $B^+ \to K^+\mu^+\mu^-$, $B^0 \to K^0\mu^+\mu^-$, $B^0 \to K^{*0}\mu^+\mu^-$ and $B^+ \to K^{*+}\mu^+\mu^-$ decays. The K^0 meson is reconstructed through the decay $K^0_S \to \pi^+\pi^-$; the K^{*+} as $K^{*+} \to K^0_S(\to \pi^+\pi^-)\pi^+$ and the K^{*0} as $K^{*0} \to K^+\pi^-$. Modes involving a K^0_L or π^0 in the final state are not considered. The individual branching fractions of $B^+ \to K^+\mu^+\mu^-$, $B^0 \to K^0\mu^+\mu^-$ and $B^+ \to K^{*+}\mu^+\mu^-$ decays are also reported. The branching fraction of the decay $B^0 \to K^{*0}\mu^+\mu^-$ has been previously reported in Ref. [10] and is not updated here.

The $B^0 \to K^{*0}\mu^+\mu^-$ and $B^+ \to K^{*+}\mu^+\mu^-$ branching fractions are influenced by the presence of $B^0 \to K^+\pi^-\mu^+\mu^-$ and $B^+ \to K^0_S\pi^+\mu^+\mu^-$ decays with the $K^+\pi^-$ or $K^0_S\pi^+$ system in a S-wave configuration. It is not possible to separate these candidates from the dominant K^{*0} and K^{*+} resonant components without performing an analysis of the $K^+\pi^-$ or $K^0_S\pi^+$ invariant mass and the angular distribution of the final state particles. The S-wave component is expected to be at the level of a few percent [11] and to cancel when evaluating the isospin asymmetry of the $B \to K^*\mu^+\mu^-$ decays.

2 Detector and dataset

The LHCb detector [12] is a single-arm forward spectrometer covering the pseudorapidity range $2 < \eta < 5$, designed for the study of particles containing b or c quarks. The detector includes a high-precision tracking system consisting of a silicon-strip vertex detector surrounding the pp interaction region, a large-area silicon-strip detector located upstream of a dipole magnet with a bending power of about 4 Tm, and three stations of silicon-strip detectors and straw drift tubes [13] placed downstream of the magnet. The combined tracking system provides a momentum measurement with relative uncertainty that varies from 0.4% at 5 GeV/c to 0.6% at 100 GeV/c, and an impact parameter resolution of 20 μm for tracks with high transverse momentum. Charged hadrons are identified using two ring-imaging Cherenkov (RICH) detectors [14]. Photon, electron and hadron candidates are identified by a calorimeter system consisting of scintillating-pad and preshower detectors, an electromagnetic calorimeter and a hadronic calorimeter. Muons are identified by a system composed of alternating layers of iron and multiwire proportional chambers [15]. Decays of $K^0_S \to \pi^+\pi^-$ are reconstructed in two different categories: the first involving K^0_S mesons that decay early enough for the daughter pions to be reconstructed in the vertex detector; and the second containing K^0_S mesons that decay later such that track segments of the pions cannot be formed in the vertex detector. These categories are referred to as *long* and *downstream*, respectively. Candidates in the long category have better mass, momentum and vertex resolution than those in the downstream category.

Simulated events are used to estimate the efficiencies of the trigger, reconstruction and subsequent event selection of the different signal decays and to estimate the contribution from specific background sources. These samples are produced using the software described in Refs. [16–22].

3 Selection

The $B \to K^{(*)}\mu^+\mu^-$ candidate events are required to pass a two-stage trigger system [23]. In the initial hardware stage, these events are selected with at least one muon with transverse momentum, $p_{\rm T} > 1.48\,(1.76)\,{\rm GeV}/c$ in 2011 (2012). In the subsequent software stage, at least one of the final-state particles is required to have $p_{\rm T} > 1.0\,{\rm GeV}/c$ and an impact parameter (IP) larger than $100\,\mu{\rm m}$ with respect to all of the primary pp interaction vertices (PVs) in the event. Finally, a multivariate algorithm [24] is used for the identification of secondary vertices consistent with the decay of a b hadron with muons in the final state.

For the $B^0 \to K^0_{\rm S}\mu^+\mu^-$ and $B^+ \to K^{*+}\mu^+\mu^-$ modes, $K^0_{\rm S}$ candidates are required to have a mass within 30 MeV/c^2 of the known $K^0_{\rm S}$ mass [25]. For the $B^0 \to K^{*0}\mu^+\mu^-$ and $B^+ \to K^{*+}\mu^+\mu^-$ modes, K^* candidates are formed by combining kaons and pions and are required to have a mass within $100\,{\rm MeV}/c^2$ of the known K^* masses [25]. For all decay modes, B candidates are formed by subsequently combining the $K^{(*)}$ meson with two muons of opposite charge and requiring the mass to be between 5170 and $5700\,{\rm MeV}/c^2$.

The event selection is common to that described in Refs. [10, 26, 27]. Signal candidates are required to pass a set of loose criteria (pre-selection) that selects candidates for further analysis if the final-state products originating directly from the B meson have an impact parameter χ^2, $\chi^2_{\rm IP} > 9$, where $\chi^2_{\rm IP}$ is defined as the minimum change in χ^2 of the vertex fit to any of the PVs in the event when the particle is added to that PV. Additionally, an associated PV is chosen based on the lowest $\chi^2_{\rm IP}$ of the B candidate. For this PV it is required that: the B candidate has $\chi^2_{\rm IP} < 16$, the vertex fit χ^2 of the PV fit must increase by more than 121 when including the B candidate daughters, and the angle between the B candidate momentum and the direction from the PV to the decay vertex is below 14 mrad. Finally, the B candidate is required to have a vertex fit $\chi^2 < 8$ per degree of freedom. For candidates containing a $K^0_{\rm S}$ meson, the $K^0_{\rm S}$ is required to have a decay time larger than 2 ps.

Using particle identification information from the RICH detectors, calorimeters and muon system, multivariate discriminants (PID variables) are employed to reject background candidates, where pions are misidentified as kaons and vice-versa, and where a pion or kaon is incorrectly identified as a muon.

The initial selection is followed by a tighter multivariate selection, based on a boosted decision tree (BDT) [28] with the AdaBoost algorithm [29], which is designed to reject background of combinatorial nature. Separate BDTs are employed for each signal decay. For decays involving a $K^0_{\rm S}$ meson, two independent BDTs are trained for the long and downstream categories. This gives a total of six BDTs which all use data from the upper mass sideband ($m(K^{(*)}\mu^+\mu^-) > 5350$ MeV/c^2) of their corresponding decay to represent the background sample in the training. Simulated $B^+ \to K^+\mu^+\mu^-$, $B^0 \to K^0_{\rm S}\mu^+\mu^-$ and $B^+ \to K^{*+}\mu^+\mu^-$ events are used as the signal sample in the training of the corresponding BDTs. In contrast, to stay consistent with the selection in Ref. [26], the signal for the training of the $B^0 \to K^{*0}\mu^+\mu^-$ BDT is taken from reconstructed $B^0 \to (J/\psi \to \mu^+\mu^-)K^{*0}$ candidates from data. Events used in the training of the BDTs are not used in the

subsequent classification of the data.

All six BDTs use predominantly geometric variables, including the variables used in the pre-selection described above. The $B^0 \to K^{*0}\mu^+\mu^-$ BDT also makes use of PID variables to further suppress background where a K^+ is misidentified as a π^+ and vice-versa in the K^{*0} decay.

The multivariate selections for $B^+ \to K^+\mu^+\mu^-$, $B^+ \to K^{*+}\mu^+\mu^-$ and $B^0 \to K^{*0}\mu^+\mu^-$ candidates have an efficiency of 90% for the signal channels and remove 95% of the background that remains after the pre-selection. The long lifetime of the K^0_S meson makes it difficult to determine whether it originates from the same vertex as the dimuon system in $B^0 \to K^0_S\mu^+\mu^-$ decays. As such, the multivariate selection for $B^0 \to K^0_S\mu^+\mu^-$ candidates has a signal efficiency of 66% and 48% for the long and downstream categories, respectively, while removing 99% of the background surviving the pre-selection.

Combinatorial background, where the final-state particles attributed to the B candidate do not all come from the same b-hadron decay, are reduced to a small level by the multivariate selection. In addition, there are several sources of background that peak in the $K^{(*)}\mu^+\mu^-$ invariant mass. The largest of these are $B \to J/\psi\, K^{(*)}$ and $B \to \psi(2S)K^{(*)}$ decays, which are rejected by removing the regions of dimuon invariant mass around the charmonium resonances ($2828 < m(\mu^+\mu^-) < 3317\,\text{MeV}/c^2$ and $3536 < m(\mu^+\mu^-) < 3873\,\text{MeV}/c^2$). A combination of mass and PID requirements remove additional peaking backgrounds. These include $\Lambda_b^0 \to \Lambda^{(*)}\mu^+\mu^-$ decays, where the proton from the $\Lambda \to p\pi^-$ decay is misidentified as a K^+ or the proton misidentified as a π^+ in the $\Lambda^* \to pK^-$ decay, $B_s^0 \to \phi\mu^+\mu^-$ decays where a kaon from $\phi \to K^+K^-$ is misidentified as a pion, and $B^+ \to K^+\mu^+\mu^-$ decays that combine with a random pion to fake a $B^0 \to K^{*0}\mu^+\mu^-$ decay. After the application of all the selection criteria the exclusive backgrounds are reduced to less than 1% of the level of the signal.

To improve the resolution on the reconstructed mass of the B meson, a kinematic fit [30] is performed for candidates involving a K^0_S meson. In the fit, the mass of the $\pi^+\pi^-$ system is constrained to the nominal K^0_S mass and the B candidate is required to originate from its associated PV.

4 Signal yield determination

Signal yields are determined using extended unbinned maximum likelihood fits to the $K^{(*)}\mu^+\mu^-$ mass in the range 5170–5700 MeV/c^2. These fits are performed in nine bins of q^2 for $B^0 \to K^0_S\mu^+\mu^-$, $B^+ \to K^{*+}\mu^+\mu^-$ and $B^0 \to K^{*0}\mu^+\mu^-$ decays, while for the $B^+ \to K^+\mu^+\mu^-$ decay the larger number of signal events allows to define nineteen q^2 bins. The binning scheme is shown in Tables 3 to 5 of the appendix. It removes the region of q^2 around the charmonium resonances. For the $B^+ \to K^+\mu^+\mu^-$ differential branching fraction, where the statistical uncertainty is the smallest, a narrow range in $m(\mu^+\mu^-)$ is also removed around the mass of the ϕ meson. The signal component in the fit is described by the sum of two Crystal Ball functions [31] with common peak values and tail parameters, but different widths. The signal shape parameters are taken from a

Table 1: Observed yields of the four signal channels summed over the q^2 bins, excluding the charmonium resonance regions. Only the statistical uncertainties are shown.

Decay mode	Signal yield
$B^+ \to K^+\mu^+\mu^-$	4746 ± 81
$B^0 \to K^0_S\mu^+\mu^-$	176 ± 17
$B^+ \to K^{*+}(\to K^0_S\pi^+)\mu^+\mu^-$	162 ± 16
$B^0 \to K^{*0}(\to K^+\pi^-)\mu^+\mu^-$	2361 ± 56

fit to $B \to J/\psi\, K^{(*)}$ channels in the data, with a correction that accounts for a small q^2 dependence on the peak value and width obtained from the simulation. The combinatorial background is parameterised by an exponential function, which is allowed to vary for each q^2 bin and K^0_S category independently. For decays involving K^0_S mesons, separate fits are made to the long and downstream categories. The mass fits for the four signal channels are shown in Fig. 1, where the long and downstream K^0_S categories are combined and the results of the fits, performed in separate q^2 bins, are merged for presentation purposes. The corresponding number of signal candidates for each channel is given in Table 1.

5 Branching fraction normalisation

Each signal mode is normalised with respect to its corresponding $B \to J/\psi\, K^{(*)}$ channel, where the J/ψ resonance decays into two muons. These normalisation channels have branching fractions that are approximately two orders of magnitude higher than those of the signal channels. Each normalisation channel has similar kinematic properties and the same final-state particles as the signal modes. This results in an almost complete cancellation of systematic uncertainties when measuring the ratio of branching fractions of the signal mode with the corresponding normalisation channel. Separate normalisations for the long and downstream K^0_S reconstruction categories are used to further cancel potential sources of systematic uncertainty.

Corrections to the IP resolution, PID variables and B candidate kinematic properties are applied to the simulated events, such that the distributions of simulated candidates from the normalisation channels agree with the data. The simulation samples are subsequently used to calculate the relative efficiencies as functions of q^2. The q^2 dependence arises mainly from trigger effects, where the muons have increased (decreased) $p_{\rm T}$ at high (low) q^2 and consequently have a higher (lower) trigger efficiency. Furthermore, at high q^2, the hadrons are almost at rest in the B meson rest frame and, like the B meson, points back to the PV in the laboratory frame. The IP requirements applied on the hadron have a lower efficiency for this region of q^2. The K^0_S channels have an additional effect due to the different acceptance of the two reconstruction categories; K^0_S mesons are more likely to be reconstructed in the long category if they have low momentum, which favours the high q^2 region. The momentum distributions of the K^0_S mesons in $B^0 \to J/\psi\, K^0_S$ and $B^+ \to J/\psi\, K^{*+}$

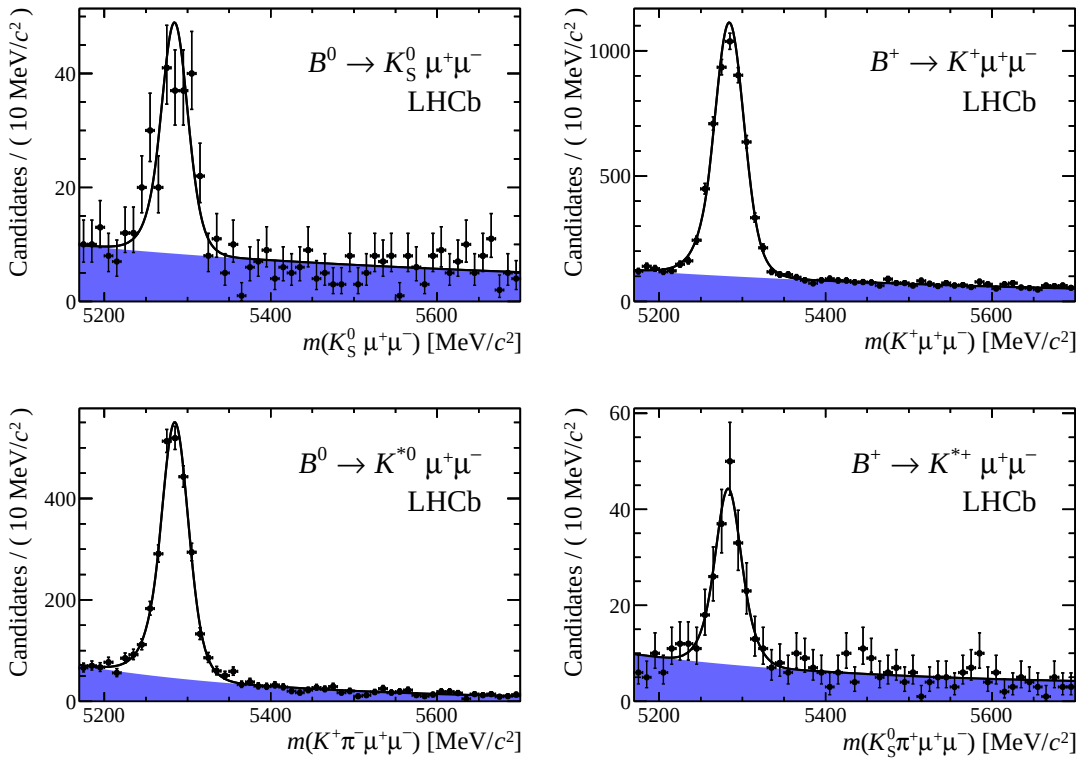

Figure 1: Reconstructed B candidate mass for the four signal modes. The data are overlaid with the result of the fit described in the text. The long and downstream K^0_S categories are combined. The results of the fits, performed in separate q^2 bins, are merged for presentation purposes. The blue (shaded) region is the combinatorial background.

decays in data and simulation for both K^0_S categories are in good agreement, indicating that the acceptance is well described in the simulation.

The measured differential branching fraction averaged over a q^2 bin of width $q^2_{\rm max} - q^2_{\rm min}$ is given by

$$\frac{d\mathcal{B}}{dq^2} = \frac{N(B\to K^{(*)}\mu^+\mu^-)}{N(B\to J/\psi\, K^{(*)})} \cdot \frac{\varepsilon(B\to J/\psi\, K^{(*)})}{\varepsilon(B\to K^{(*)}\mu^+\mu^-)} \cdot \frac{\mathcal{B}(B\to J/\psi\, K^{(*)})\mathcal{B}(J/\psi\,\to \mu^+\mu^-)}{(q^2_{\rm max} - q^2_{\rm min})}, \quad (2)$$

where $N(B\to K^{(*)}\mu^+\mu^-)$ is the number of signal candidates in the bin, $N(B\to J/\psi\, K^{(*)})$ is the number of normalisation candidates, the product of $\mathcal{B}(B\to J/\psi\, K^{(*)})$ and $\mathcal{B}(J/\psi\,\to \mu^+\mu^-)$ is the visible branching fraction of the normalisation channel, and $\varepsilon(B\to K^{(*)}\mu^+\mu^-)/\varepsilon(B\to J/\psi\, K^{(*)})$ is the relative efficiency between the signal and normalisation channels in the bin.

6 Systematic uncertainties

The branching fraction measurements of the normalisation modes from the B-factory experiments assume that the B^+ and B^0 mesons are produced with equal proportions at the $\Upsilon(4S)$ resonance [32–34]. In contrast, in this paper isospin symmetry is assumed for the $B \to J/\psi\, K^{(*)}$ decays, implying that the $B^+ \to J/\psi\, K^+$ ($B^+ \to J/\psi\, K^{*+}$) and $B^0 \to J/\psi\, K^0$ ($B^0 \to J/\psi\, K^{*0}$) decays have the same partial width. The branching fractions used in the normalisation are obtained by: taking the most precise branching fraction results from Ref. [32] and translating them into partial widths; averaging the partial widths of the K^+, K^0 and the K^{*+}, K^{*0} modes, respectively; and finally translating the widths back to branching fractions. The calculation only requires knowledge of the ratio of B^0 and B^+ lifetimes for which we use 0.93 ± 0.01 [25]. Statistical uncertainties are treated as uncorrelated while systematical uncertainties are conservatively treated as fully correlated. The resulting branching fractions of the normalisation channels are

$$\begin{aligned}
\mathcal{B}(B^+ \to J/\psi\, K^+) &= (0.998 \pm 0.014 \pm 0.040) \times 10^{-3}, \\
\mathcal{B}(B^0 \to J/\psi\, K^0) &= (0.928 \pm 0.013 \pm 0.037) \times 10^{-3}, \\
\mathcal{B}(B^+ \to J/\psi\, K^{*+}) &= (1.431 \pm 0.027 \pm 0.090) \times 10^{-3}, \\
\mathcal{B}(B^0 \to J/\psi\, K^{*0}) &= (1.331 \pm 0.025 \pm 0.084) \times 10^{-3},
\end{aligned}$$

where the first uncertainty is statistical and the second systematic. The uncertainties on the branching fractions of the normalisation modes constitute the dominant source of systematic uncertainty on the branching fraction measurements while it cancels in the isospin measurements.

A systematic uncertainty is assigned to account for the imperfect knowledge of the q^2 spectrum in the simulation within each q^2 bin. For example, the recent observation of a resonance in the high q^2 region of $B^+ \to K^+\mu^+\mu^-$ decays [26] alters the q^2 distribution and hence the selection efficiencies in that region. By reweighting simulated events to account for this resonance, and for variations of the $B \to K^{(*)}$ form factor model, a systematic uncertainty is determined at the level of $(1-2)\%$ depending on channel and q^2 bin.

Data-driven corrections of the long and downstream tracking efficiencies in the simulation are determined using *tag-and-probe* techniques in $J/\psi \to \mu^+\mu^-$ and $D^0 \to \phi K^0_{\rm S}$ decays, respectively. These techniques require that one of the particles, the *tag*, is fully reconstructed and the other, the *probe*, is only partially reconstructed. For the first decay, one of the two muons in the J/ψ decay act as the tag and the other as the probe while in the second decay the pions from the $K^0_{\rm S}$ decay are used. The method allows for an unbiased measurement of the reconstruction efficiency. The resulting systematic uncertainty on the efficiency ratio, due to finite precision of the measurement, is found to be negligible. The systematic uncertainty that arises from the corrections to the IP resolution, PID variables and B candidate kinematic properties in the simulation varies between 1% and 3% depending on channel and q^2 bin.

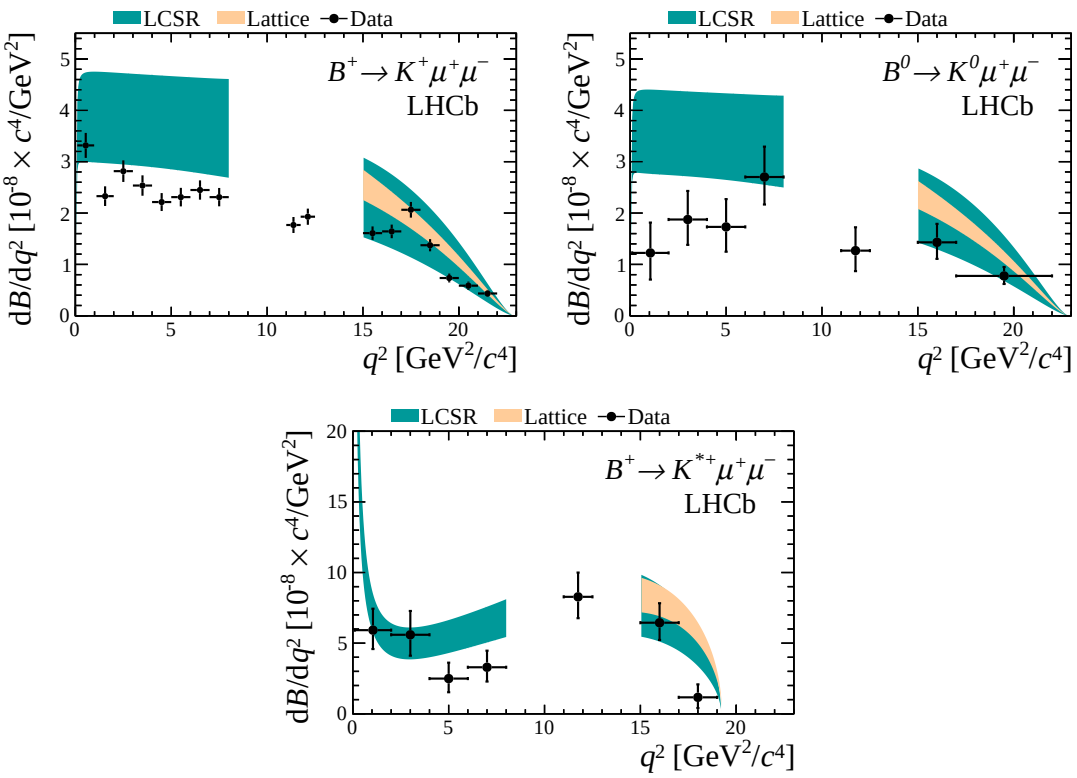

Figure 2: Differential branching fraction results for the $B^+ \to K^+\mu^+\mu^-$, $B^0 \to K^0\mu^+\mu^-$ and $B^+ \to K^{*+}\mu^+\mu^-$ decays. The uncertainties shown on the data points are the quadratic sum of the statistical and systematic uncertainties. The shaded regions illustrate the theoretical predictions and their uncertainties from light cone sum rule and lattice QCD calculations.

7 Branching fraction results

The differential branching fraction results for $B^+ \to K^+\mu^+\mu^-$, $B^0 \to K^0\mu^+\mu^-$ and $B^+ \to K^{*+}\mu^+\mu^-$ decays are shown in Fig. 2 with theoretical predictions [35, 36] superimposed. The values are given in Tables 3 to 5 in the appendix. In the low q^2 region, these predictions rely on the QCD factorisation approaches from Refs. [37,38] for $B \to K^*\mu^+\mu^-$ and Ref. [39] for $B \to K\mu^+\mu^-$, and lose accuracy when approaching the J/ψ resonance. In the high q^2 region, an operator product expansion in the inverse b-quark mass, $1/m_b$, and in $1/\sqrt{q^2}$ is used based on Ref. [40]. This expansion is only valid above the open charm threshold. A dimensional estimate of the uncertainty associated with this expansion is discussed in Ref. [41]. For light cone sum rule (LCSR) predictions, the $B \to K^{(*)}$ form factor calculations are taken from Refs. [42] and [43]. Predictions based on form factors from lattice calculations are also overlaid [1, 2, 44, 45].

Although all three differential branching fraction measurements are consistent with the SM, they all have values smaller than the theoretical prediction. The sample size for $B^+ \to K^+\mu^+\mu^-$ is sufficient to show significant structures in the q^2 distribution. As an

Table 2: Integrated branching fractions (10^{-8}) in the high q^2 region. For the $B \to K\mu^+\mu^-$ modes the region is defined as $15 - 22\,\mathrm{GeV}^2/c^4$, while for $B^+ \to K^{*+}\mu^+\mu^-$ it is $15 - 19\,\mathrm{GeV}^2/c^4$. Predictions are obtained using the form factors calculated in lattice QCD over the same q^2 regions. For the measurements, the first uncertainty is statistical and the second systematic.

Decay mode	Measurement	Prediction
$B^+ \to K^+\mu^+\mu^-$	$8.5 \pm 0.3 \pm 0.4$	10.7 ± 1.2
$B^0 \to K^0\mu^+\mu^-$	$6.7 \pm 1.1 \pm 0.4$	9.8 ± 1.0
$B^+ \to K^{*+}\mu^+\mu^-$	$15.8\ ^{+3.2}_{-2.9} \pm 1.1$	26.8 ± 3.6

example, the peak at high q^2 is due to the $\psi(4160)$ resonance, which is discussed in more detail in Ref. [26].

The presence of an S-wave contribution to the $K^+\pi^-$ and $K^0_S\pi^+$ systems of $B^0 \to K^{*0}\mu^+\mu^-$ and $B^+ \to K^{*+}\mu^+\mu^-$ candidates, respectively, complicates the analysis of these channels. This effect is of the order of a few percent and can be neglected in $B^+ \to K^{*+}\mu^+\mu^-$ decays with the current statistical precision. The larger signal yield of $B^0 \to K^{*0}\mu^+\mu^-$, however, merits a detailed analysis of the S-wave contribution and requires a dedicated study. For this reason the branching fraction of $B^0 \to K^{*0}\mu^+\mu^-$ decays is not reported.

By convention, branching fractions are extrapolated to the full q^2 range ignoring the presence of the narrow charmonium resonances. A q^2 distribution based on Ref. [46] is used for this. The correction factors to the branching fractions due to this extrapolation are 1.39 and 1.50 for $B \to K\mu^+\mu^-$ and $B^0 \to K^{*0}\mu^+\mu^-$, respectively. No uncertainty is assigned to these corrections. Summing the q^2 bins and applying the extrapolation, the integrated branching fractions become

$$\begin{aligned}
\mathcal{B}(B^+ \to K^+\mu^+\mu^-) &= (4.29 \pm 0.07\,(\mathrm{stat}) \pm 0.21\,(\mathrm{syst})) \times 10^{-7},\\
\mathcal{B}(B^0 \to K^0\mu^+\mu^-) &= (3.27 \pm 0.34\,(\mathrm{stat}) \pm 0.17\,(\mathrm{syst})) \times 10^{-7},\\
\mathcal{B}(B^+ \to K^{*+}\mu^+\mu^-) &= (9.24 \pm 0.93\,(\mathrm{stat}) \pm 0.67\,(\mathrm{syst})) \times 10^{-7}.
\end{aligned}$$

These measurements are more precise than the current world averages [25].

Table 2 compares the $B^+ \to K^+\mu^+\mu^-$ and $B^0 \to K^0\mu^+\mu^-$ branching fractions integrated over the q^2 region of $15{-}22\,\mathrm{GeV}^2/c^4$, and the $B^+ \to K^{*+}\mu^+\mu^-$ branching fraction integrated over the $15 - 19\,\mathrm{GeV}^2/c^4$ region to the lattice QCD predictions [1, 2, 44, 45]. While the measurements are all individually consistent with their respective predictions, they all have values below those.

8 Isospin asymmetry results

The assumption of no isospin asymmetry in the $B \to J/\psi\,K^{(*)}$ modes makes the isospin measurement equivalent to measuring the difference in isospin asymmetry between $B \to K^{(*)}\mu^+\mu^-$ and $B \to J/\psi\,K^{(*)}$ decays. Compared to using the values in Ref. [25] for the branching fractions of the $B \to J/\psi\,K^{(*)}$ modes, this approach shifts A_I in each bin by

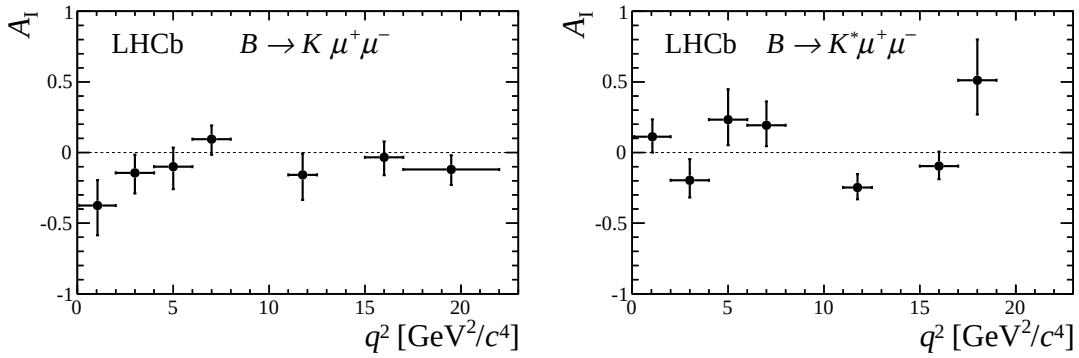

Figure 3: Isospin asymmetries for (left) $B \to K\mu^+\mu^-$ and (right) $B \to K^*\mu^+\mu^-$ decays.

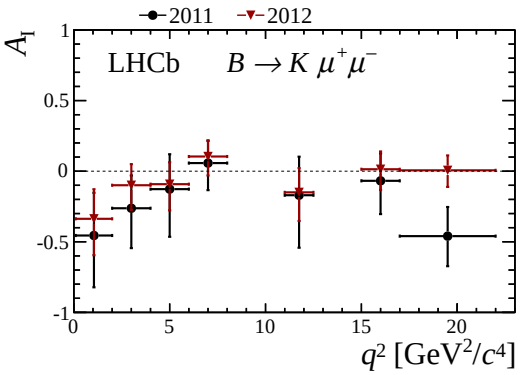

Figure 4: Isospin asymmetry of $B \to K\mu^+\mu^-$ obtained separately from the 2011 and 2012 data sets.

approximately 4%. The isospin asymmetries are shown in Fig. 3 for $B \to K\mu^+\mu^-$ and $B \to K^*\mu^+\mu^-$ and given in Tables 6 and 7 in the appendix. The asymmetric uncertainties are obtained from the profile likelihood.

Since there is no knowledge on the shape of A_I in models that extend the SM, apart from large correlations expected between neighbouring bins, the $A_I = 0$ hypothesis is tested against the simplest alternative, that is a constant value different from zero. The difference in χ^2 between the two hypotheses is used as a test statistic and is compared to the differences in an ensemble of pseudo-experiments which are generated with zero isospin asymmetry. Given the current statistical precision, the hypothesis of $A_I = 0$ is a good approximation to the SM which predicts A_I to be $\mathcal{O}(1\%)$ [3–5]. The p-value for the $B \to K\mu^+\mu^-$ isospin asymmetry under the $A_I = 0$ hypothesis is 11%, corresponding to a significance of $1.5\,\sigma$. The $B \to K^*\mu^+\mu^-$ isospin asymmetry has a p-value of 80% with respect to zero. Alternatively, a simple χ^2 test of the data with respect to a hypothesis of zero isospin asymmetry has a p-value of 54% (4%) for the $B \to K\mu^+\mu^-$ ($B \to K^*\mu^+\mu^-$) isospin asymmetry.

Although the isospin asymmetry for $B \to K\mu^+\mu^-$ decays is negative in all but one q^2

bin, results are more consistent with the SM compared to the previous measurement in Ref. [9], which quoted a $4.4\,\sigma$ significance to differ from zero, using a test statistic that explicitly tested for $A_{\rm I}$ to be negative in all bins. The lower significance quoted here is due to four effects: the change of the test statistic in the calculation of the significance itself, which reduces the previous discrepancy to $3.5\,\sigma$; the assumption that the isospin asymmetry of $B \to J/\psi\, K^{(*)}$ is zero which reduces the significance further to $3.2\,\sigma$; a re-analysis of the 2011 data with the updated reconstruction and event selection that reduces the significance to $2.5\,\sigma$; and finally the inclusion of the 2012 data set reduces the significance further to $1.5\,\sigma$.

The measurements of $A_{\rm I}$ in the individual q^2 bins obtained from the re-analysis of the 2011 data set are compatible with those obtained in the previous analysis; a χ^2 test on the compatibility of the two results, taking the overlap of events into account, has a p-value of 93%. However results from the 2012 data are more compatible with an $A_{\rm I}$ value of zero than the re-analysed 2011 data, as shown in Fig 4.

9 Conclusion

The most precise measurements of the differential branching fractions of $B^+ \to K^+\mu^+\mu^-$, $B^0 \to K^0_{\rm S}\mu^+\mu^-$ and $B^+ \to K^{*+}\mu^+\mu^-$ decays as well as the isospin asymmetries of $B \to K\mu^+\mu^-$ and $B \to K^*\mu^+\mu^-$ decays have been performed using a data set corresponding to $3\,{\rm fb}^{-1}$ of integrated luminosity collected by the LHCb detector.

The isospin asymmetries of the $B \to K\mu^+\mu^-$ and $B \to K^*\mu^+\mu^-$ decays are both consistent with SM expectations. However, the branching fraction measurements all have lower values than the SM predictions. This is consistent with the $B^0 \to K^{*0}\mu^+\mu^-$ and $B^0_s \to \phi\mu^+\mu^-$ branching fractions measured by LHCb, which also favour lower values [10, 45, 47] than predicted by the SM.

Acknowledgements

We would like to thank Roman Zwicky for the useful discusions regarding $A_{\rm I}$ in the $B \to J/\psi\, K^{(*)}$ system, and Chris Bouchard and Stefan Meinel for information on branching fraction predictions of $B \to K\mu^+\mu^-$ and $B \to K^*\mu^+\mu^-$ from the lattice calculations. We express our gratitude to our colleagues in the CERN accelerator departments for the excellent performance of the LHC. We thank the technical and administrative staff at the LHCb institutes. We acknowledge support from CERN and from the national agencies: CAPES, CNPq, FAPERJ and FINEP (Brazil); NSFC (China); CNRS/IN2P3 and Region Auvergne (France); BMBF, DFG, HGF and MPG (Germany); SFI (Ireland); INFN (Italy); FOM and NWO (The Netherlands); SCSR (Poland); MEN/IFA (Romania); MinES, Rosatom, RFBR and NRC "Kurchatov Institute" (Russia); MinECo, XuntaGal and GENCAT (Spain); SNSF and SER (Switzerland); NASU (Ukraine); STFC and the Royal Society (United Kingdom); NSF (USA). We also acknowledge the support received from EPLANET, Marie Curie Actions and the ERC under FP7. The Tier1 computing

centres are supported by IN2P3 (France), KIT and BMBF (Germany), INFN (Italy), NWO and SURF (The Netherlands), PIC (Spain), GridPP (United Kingdom). We are indebted to the communities behind the multiple open source software packages on which we depend. We are also thankful for the computing resources and the access to software R&D tools provided by Yandex LLC (Russia).

References

[1] C. Bouchard *et al.*, *Rare decay $B \to K\ell^+\ell^-$ form factors from lattice QCD*, Phys. Rev. **D88** (2013) 054509, arXiv:1306.2384.

[2] R. R. Horgan, Z. Liu, S. Meinel, and M. Wingate, *Lattice QCD calculation of form factors describing the rare decays $B \to K^*\ell^+\ell^-$ and $B_s \to \phi\ell^+\ell^-$*, arXiv:1310.3722.

[3] T. Feldmann and J. Matias, *Forward-backward and isospin asymmetry for $B \to K^{(*)}\ell^+\ell^-$ decay in the standard model and in supersymmetry*, JHEP **01** (2003) 074, arXiv:hep-ph/0212158.

[4] A. Khodjamirian, T. Mannel, and Y. Wang, *$B \to K\ell^+\ell^-$ decay at large hadronic recoil*, JHEP **02** (2013) 010, arXiv:1211.0234.

[5] J. Lyon and R. Zwicky, *Isospin asymmetries in $B \to (K^*, \rho)\gamma/l^+l^-$ and $B \to Kl^+l^-$ in and beyond the standard model*, Phys. Rev. **D88** (2013) 094004, arXiv:1305.4797.

[6] Heavy Flavor Averaging Group, Y. Amhis *et al.*, *Averages of b-hadron, c-hadron, and τ-lepton properties as of early 2012*, arXiv:1207.1158, updated results and plots available at http://www.slac.stanford.edu/xorg/hfag/.

[7] BaBar collaboration, B. Aubert *et al.*, *Measurement of branching fractions and rate asymmetries in the rare decays $B \to K^{(*)}\ell^+\ell^-$*, Phys. Rev. **D86** (2012) 032012, arXiv:hep-ex/1204.3933.

[8] Belle collaboration, J.-T. Wei *et al.*, *Measurement of the differential branching fraction and forward-backward asymmetry for $B \to K^{(*)}l^+l^-$*, Phys. Rev. Lett. **103** (2009) 171801, arXiv:0904.0770.

[9] LHCb collaboration, R. Aaij *et al.*, *Measurement of the isospin asymmetry in $B \to K^{(*)}\mu^+\mu^-$ decays*, JHEP **07** (2012) 133, arXiv:1205.3422.

[10] LHCb collaboration, R. Aaij *et al.*, *Differential branching fraction and angular analysis of the decay $B^0 \to K^{*0}\mu^+\mu^-$*, JHEP **08** (2013) 131, arXiv:1304.6325.

[11] D. Becirevic and A. Tayduganov, *Impact of $B \to K_0^*\ell^+\ell^-$ on the New Physics search in $B \to K^*\ell^+\ell^-$ decay*, Nucl. Phys. **B868** (2013) 368, arXiv:1207.4004.

[12] LHCb collaboration, A. A. Alves Jr. *et al.*, *The LHCb detector at the LHC*, JINST **3** (2008) S08005.

[13] R. Arink *et al.*, *Performance of the LHCb Outer Tracker*, arXiv:1311.3893, submitted to JINST.

[14] F. Archilli *et al.*, *Performance of the muon identification at LHCb*, JINST **8** (2013) P10020, arXiv:1306.0249.

[15] M. Adinolfi *et al.*, *Performance of the LHCb RICH detector at the LHC*, Eur. Phys. J. **C73** (2013) 2431, arXiv:1211.6759.

[16] T. Sjöstrand, S. Mrenna, and P. Skands, *PYTHIA 6.4 Physics and manual*, JHEP **05** (2006) 026, arXiv:hep-ph/0603175.

[17] T. Sjöstrand, S. Mrenna, and P. Skands, *A brief introduction to PYTHIA 8.1*, Comput. Phys. Commun. **178** (2008) 852, arXiv:0710.3820.

[18] I. Belyaev *et al.*, *Handling of the generation of primary events in* Gauss*, the LHCb simulation framework*, Nuclear Science Symposium Conference Record (NSS/MIC) **IEEE** (2010) 1155.

[19] D. J. Lange, *The EvtGen particle decay simulation package*, Nucl. Instrum. Meth. **A462** (2001) 152.

[20] P. Golonka and Z. Was, *PHOTOS Monte Carlo: a precision tool for QED corrections in Z and W decays*, Eur. Phys. J. **C45** (2006) 97, arXiv:hep-ph/0506026.

[21] GEANT4 collaboration, J. Allison *et al.*, *Geant4 developments and applications*, IEEE Trans. Nucl. Sci. **53** (2006) 270; GEANT4 collaboration, S. Agostinelli *et al.*, *GEANT4: A simulation toolkit*, Nucl. Instrum. Meth. **A506** (2003) 250.

[22] M. Clemencic *et al.*, *The LHCb simulation application, Gauss: design, evolution and experience*, J. of Phys: Conf. Ser. **331** (2011) 032023.

[23] R. Aaij *et al.*, *The LHCb trigger and its performance in 2011*, JINST **8** (2013) P04022, arXiv:1211.3055.

[24] V. V. Gligorov and M. Williams, *Efficient, reliable and fast high-level triggering using a bonsai boosted decision tree*, JINST **8** (2013) P02013, arXiv:1210.6861.

[25] Particle Data Group, J. Beringer *et al.*, *Review of particle physics*, Phys. Rev. **D86** (2012) 010001, and 2013 partial update for the 2014 edition.

[26] LHCb collaboration, R. Aaij *et al.*, *Observation of a resonance in $B^+ \to K^+\mu^+\mu^-$ decays at low recoil*, Phys. Rev. Lett. **111** (2013) 112003, arXiv:1307.7595.

[27] LHCb collaboration, R. Aaij *et al.*, *Angular analysis of charged and neutral $B \to K\mu^+\mu^-$ decays*, LHCb-PAPER-2014-007, in preparation.

[28] L. Breiman, J. H. Friedman, R. A. Olshen, and C. J. Stone, *Classification and regression trees*. Wadsworth international group, Belmont, California, USA, 1984.

[29] R. E. Schapire and Y. Freund, *A decision-theoretic generalization of on-line learning and an application to boosting*, Jour. Comp. and Syst. Sc. **55** (1997) 119.

[30] W. D. Hulsbergen, *Decay chain fitting with a Kalman filter*, Nucl. Instrum. Meth. **A552** (2005) 566, arXiv:physics/0503191.

[31] T. Skwarnicki, *A study of the radiative cascade transitions between the Upsilon-prime and Upsilon resonances*, PhD thesis, Institute of Nuclear Physics, Krakow, 1986, DESY-F31-86-02.

[32] BaBar collaboration, B. Aubert *et al.*, *Measurement of branching fractions and charge asymmetries for exclusive B decays to charmonium*, Phys. Rev. Lett. **94** (2005) 141801, arXiv:hep-ex/0412062.

[33] Belle collaboration, K. Abe *et al.*, *Measurement of branching fractions and charge asymmetries for two-body B meson decays with charmonium*, Phys. Rev. **D67** (2003) 032003, arXiv:hep-ex/0211047.

[34] Belle collaboration, K. Abe *et al.*, *Measurements of branching fractions and decay amplitudes in $B \to J/\psi K^*$ decays*, Phys. Lett. **B538** (2002) 11, arXiv:hep-ex/0205021.

[35] C. Bobeth, G. Hiller, and D. van Dyk, *More benefits of semileptonic rare B decays at low recoil: CP Violation*, JHEP **07** (2011) 067, arXiv:1105.0376.

[36] C. Bobeth, G. Hiller, D. van Dyk, and C. Wacker, *The decay $B \to K\ell^+\ell^-$ at low hadronic recoil and model-independent $\Delta B = 1$ constraints*, JHEP **01** (2012) 107, arXiv:1111.2558.

[37] M. Beneke, T. Feldmann, and D. Seidel, *Systematic approach to exclusive $B \to V\ell^+\ell^-$, $V\gamma$ decays*, Nucl. Phys. **B612** (2001) 25, arXiv:hep-ph/0106067.

[38] M. Beneke, T. Feldmann, and D. Seidel, *Exclusive radiative and electroweak $b \to d$ and $b \to s$ penguin decays at NLO*, Eur. Phys. J. **C41** (2005) 173, arXiv:hep-ph/0412400.

[39] C. Bobeth, G. Hiller, and G. Piranishvili, *Angular distributions of $\bar{B} \to K\bar{\ell}\ell$ decays*, JHEP **12** (2007) 040, arXiv:0709.4174.

[40] B. Grinstein and D. Pirjol, *Exclusive rare $B \to K^*\ell^+\ell^-$ decays at low recoil: controlling the long-distance effects*, Phys. Rev. **D70** (2004) 114005, arXiv:hep-ph/0404250.

[41] U. Egede *et al.*, *New observables in the decay mode $\overline{B}{}^0_d \to \overline{K}{}^{*0}\ell^+\ell^-$*, JHEP **11** (2008) 032, arXiv:0807.2589.

[42] P. Ball and R. Zwicky, *$B_{d,s} \to \rho$, ω, K^*, ϕ decay form factors from light-cone sum rules reexamined*, Phys. Rev. **D71** (2005) 014029, arXiv:hep-ph/0412079.

[43] A. Khodjamirian, T. Mannel, A. Pivovarov, and Y.-M. Wang, *Charm-loop effect in $B \to K^{(*)}\ell^+\ell^-$ and $B \to K^*\gamma$*, JHEP **09** (2010) 089, arXiv:1006.4945.

[44] C. Bouchard *et al.*, *Standard model predictions for $B \to K\ell^+\ell^-$ with form factors from lattice QCD*, Phys. Rev. Lett. **111** (2013) 162002, arXiv:1306.0434.

[45] R. R. Horgan, Z. Liu, S. Meinel, and M. Wingate, *Calculation of $B \to K^*\mu^+\mu^-$ and $B_s \to \phi\mu^+\mu^-$ using form factors from lattice QCD*, arXiv:1310.3887.

[46] A. Ali, P. Ball, L. T. Handoko, and G. Hiller, *Comparative study of the decays $B \to (K, K^*)\ell^+\ell^-$ in the standard model and supersymmetric theories*, Phys. Rev. **D61** (2000) 074024, arXiv:hep-ph/9910221.

[47] LHCb collaboration, R. Aaij *et al.*, *Differential branching fraction and angular analysis of the decay $B_s^0 \to \phi\mu^+\mu^-$*, JHEP **07** (2013) 84, arXiv:1305.2168.

A Appendix

Table 3: Differential branching fraction results ($10^{-9} \times c^4/\mathrm{GeV}^2$) for the $B^+ \to K^+\mu^+\mu^-$ decay, including statistical and systematic uncertainties.

q^2 range (GeV^2/c^4)	central value	stat	syst
$0.1 < q^2 < 0.98$	33.2	1.8	1.7
$1.1 < q^2 < 2.0$	23.3	1.5	1.2
$2.0 < q^2 < 3.0$	28.2	1.6	1.4
$3.0 < q^2 < 4.0$	25.4	1.5	1.3
$4.0 < q^2 < 5.0$	22.1	1.4	1.1
$5.0 < q^2 < 6.0$	23.1	1.4	1.2
$6.0 < q^2 < 7.0$	24.5	1.4	1.2
$7.0 < q^2 < 8.0$	23.1	1.4	1.2
$11.0 < q^2 < 11.8$	17.7	1.3	0.9
$11.8 < q^2 < 12.5$	19.3	1.2	1.0
$15.0 < q^2 < 16.0$	16.1	1.0	0.8
$16.0 < q^2 < 17.0$	16.4	1.0	0.8
$17.0 < q^2 < 18.0$	20.6	1.1	1.0
$18.0 < q^2 < 19.0$	13.7	1.0	0.7
$19.0 < q^2 < 20.0$	7.4	0.8	0.4
$20.0 < q^2 < 21.0$	5.9	0.7	0.3
$21.0 < q^2 < 22.0$	4.3	0.7	0.2
$1.1 < q^2 < 6.0$	24.2	0.7	1.2
$15.0 < q^2 < 22.0$	12.1	0.4	0.6

Table 4: Differential branching fraction results ($10^{-9} \times c^4/\mathrm{GeV}^2$) for the $B^0 \to K^0\mu^+\mu^-$ decay, including statistical and systematic uncertainties.

q^2 range (GeV^2/c^4)	central value	stat	syst
$0.1 < q^2 < 2.0$	12.2	$^{+5.9}_{-5.2}$	0.6
$2.0 < q^2 < 4.0$	18.7	$^{+5.5}_{-4.9}$	0.9
$4.0 < q^2 < 6.0$	17.3	$^{+5.3}_{-4.8}$	0.9
$6.0 < q^2 < 8.0$	27.0	$^{+5.8}_{-5.3}$	1.4
$11.0 < q^2 < 12.5$	12.7	$^{+4.5}_{-4.0}$	0.6
$15.0 < q^2 < 17.0$	14.3	$^{+3.5}_{-3.2}$	0.7
$17.0 < q^2 < 22.0$	7.8	$^{+1.7}_{-1.5}$	0.4
$1.1 < q^2 < 6.0$	18.7	$^{+3.5}_{-3.2}$	0.9
$15.0 < q^2 < 22.0$	9.5	$^{+1.6}_{-1.5}$	0.5

Table 5: Differential branching fraction results ($10^{-9} \times c^4/\mathrm{GeV}^2$) for the $B^+ \to K^{*+}\mu^+\mu^-$ decay, including statistical and systematic uncertainties.

q^2 range (GeV^2/c^4)	central value	stat	syst
$0.1 < q^2 < 2.0$	59.2	$^{+14.4}_{-13.0}$	4.0
$2.0 < q^2 < 4.0$	55.9	$^{+15.9}_{-14.4}$	3.8
$4.0 < q^2 < 6.0$	24.9	$^{+11.0}_{-\ 9.6}$	1.7
$6.0 < q^2 < 8.0$	33.0	$^{+11.3}_{-\ 10.0}$	2.3
$11.0 < q^2 < 12.5$	82.8	$^{+15.8}_{-14.1}$	5.6
$15.0 < q^2 < 17.0$	64.4	$^{+12.9}_{-11.5}$	4.4
$17.0 < q^2 < 19.0$	11.6	$^{+\ 9.1}_{-\ 7.6}$	0.8
$1.1 < q^2 < 6.0$	36.6	$^{+\ 8.3}_{-\ 7.6}$	2.6
$15 < q^2 < 19.0$	39.5	$^{+\ 8.0}_{-\ 7.3}$	2.8

Table 6: Isospin asymmetry results for the $B \to K\mu^+\mu^-$ decay, including statistical and systematic uncertainties.

q^2 range (GeV$^2/c^4$)	central value	stat	syst
$0.1 < q^2 < 2.0$	-0.37	$^{+0.18}_{-0.21}$	0.02
$2.0 < q^2 < 4.0$	-0.15	$^{+0.13}_{-0.15}$	0.02
$4.0 < q^2 < 6.0$	-0.10	$^{+0.13}_{-0.16}$	0.02
$6.0 < q^2 < 8.0$	0.09	$^{+0.10}_{-0.11}$	0.02
$11.0 < q^2 < 12.5$	-0.16	$^{+0.15}_{-0.18}$	0.03
$15.0 < q^2 < 17.0$	-0.04	$^{+0.11}_{-0.13}$	0.02
$17.0 < q^2 < 22.0$	-0.12	$^{+0.10}_{-0.11}$	0.02
$1.1 < q^2 < 6.0$	-0.10	$^{+0.08}_{-0.09}$	0.02
$15.0 < q^2 < 22.0$	-0.09	$^{+0.08}_{-0.08}$	0.02

Table 7: Isospin asymmetry results for the $B \to K^*\mu^+\mu^-$ decay, including statistical and systematic uncertainties.

q^2 range (GeV$^2/c^4$)	central value	stat	syst
$0.1 < q^2 < 2.0$	0.11	$^{+0.12}_{-0.11}$	0.02
$2.0 < q^2 < 4.0$	-0.20	$^{+0.15}_{-0.12}$	0.03
$4.0 < q^2 < 6.0$	0.23	$^{+0.21}_{-0.18}$	0.02
$6.0 < q^2 < 8.0$	0.19	$^{+0.17}_{-0.15}$	0.02
$11.0 < q^2 < 12.5$	-0.25	$^{+0.09}_{-0.08}$	0.03
$15.0 < q^2 < 17.0$	-0.10	$^{+0.10}_{-0.09}$	0.03
$17.0 < q^2 < 19.0$	0.51	$^{+0.29}_{-0.24}$	0.02
$1.1 < q^2 < 6.0$	0.00	$^{+0.12}_{-0.10}$	0.02
$15.0 < q^2 < 19.0$	0.06	$^{+0.10}_{-0.09}$	0.02